Cytotechnology (2006) 51:7–19
DOI 10.1007/s10616-006-9006-7

ORIGINAL PAPER

Automated time-lapse microscopy and high-resolution tracking of cell migration

Joseph S. Fotos · Vivek P. Patel · Norman J. Karin · Murali K. Temburni · John T. Koh · Deni S. Galileo

Received: 18 January 2006 / Accepted: 3 April 2006 / Published online: 8 August 2006

Abstract We describe a novel fully automated high-throughput time-lapse microscopy system and evaluate its performance for precisely tracking the motility of several glioma and osteoblastic cell lines. Use of this system revealed cell motility behavior not discernable with conventional techniques by collecting data (1) from closely spaced time points (minutes), (2) over long periods (hours to days), (3) from multiple areas of interest, (4) in parallel under several different experimental conditions. Quantitation of true individual and average cell velocity and path length was obtained with high spatial and temporal resolution in ''scratch'' or ''wound healing'' assays. This revealed unique motility dynamics of drug-treated and adhesion molecule-transfected cells and, thus, this is a considerable improvement over current methods of measurement and analysis. Several fluorescent vital labeling methods commonly used for end-point analyses (GFP expression, DiO lipophilic dye, and Qtracker nanocrystals) were found to be useful for time-lapse studies under specific conditions that are described. To illustrate one application, fluorescently labeled tumor cells were seeded onto cell monolayers expressing ectopic adhesion molecules, and this resulted in consistently reduced tumor cell migration velocities. These highly quantitative time-lapse analysis methods will promote the creation of new cell motility assays and increase the resolution and accuracy of existing assays.

Keywords Cell migration · Green fluorescent protein · Scratch assay · Time-lapse · Tumor cell lines · Vital fluorescent labeling

Joseph S. Fotos and Vivek P. Patel contributed equally to this work

J. S. Fotos · V. P. Patel · N. J. Karin · M. K. Temburni · D. S. Galileo (✉)
Department of Biological Sciences, University of Delaware, Wolf Hall, Newark, DE 19716, USA
e-mail: dgalileo@udel.edu

J. T. Koh · M. K. Temburni
Chemistry and Biochemistry, University of Delaware, Newark, DE 19716, USA

N. J. Karin
Pacific Northwest National Laboratory, 902 Battelle Blvd., Richland, WA 99352, USA

Introduction

Analysis of cell migratory behavior in vitro in response to chemical agents, genetic manipulations, or molecule-coated surfaces is used to dissect mechanisms that occur during development, normal physiological responses, or abnormal pathological conditions (Gavert et al. 2005; Petridis et al. 2004; Nishio et al. 2005; Yoshida

et al. 2004; Zhang et al. 2005; Herren et al. 2001; Lee et al. 2004; Maschler et al. 2005; Zhu et al. 2004; Moyano et al. 2003). Many analyses, however, lack ability to analyze individual cells, precision of measurements, or temporal resolution. Sometimes, analyses are limited to single distance measurements of a cell ''front'' at the end point of an experiment. Automated systems often require specific chambers or dishes that limit the types of experiments that can be done. Thus, most questions that are addressed in current cell motility studies are constrained by technical limitations.

One simple and widely used cell migration assay that can be done without complicated instrumentation is the ''scratch'' or ''wound healing'' assay (Endo et al. 2005; Motegi et al. 2003; Pratt et al. 2005; Wadham et al. 2003; Besson et al. 2004). For this, an instrument such as a pipettor tip is used to scrape a linear interruption in a confluent or subconfluent cell monolayer, after which cells at the edge migrate into the denuded area. Measurements from micrographs are made either of linear distances between the scratch edges or of cell densities into the denuded areas at a single or a few time points after scratching. These are believed to provide a reasonable measurement of the average migration of the cells under study, and have shown differences under experimental treatments. Differences in measurements are used to make conclusions about the effects of experimental manipulations on cell migration distances and rates. Sometimes, however, measurements are not taken, and conclusions are based on qualitative inspection of the scratched area.

Here, we describe a highly quantitative approach to measurements of the scratch assay and random cell motility under different experimental treatments using automated time-lapse microscopy. In each case, a small population of individual cells was tracked through closely spaced time intervals over approximately 20 h using commercial tracking software designed for subcellular objects. This allowed accurate average distances and velocities to be calculated and plotted with high resolution. Conventional distance measurements in the scratch assay were found to be substantial over-estimates compared to averages for tracked cell populations. Treatments sometimes resulted in changes of migration velocity during the experiment that would have been overlooked by conventional approaches. We also evaluated different methods of vital fluorescent labeling and applied this to tracking tumor cells on cell monolayers, and were successful in this by demonstrating the effect on motility of a single cell surface adhesion molecule. Details are provided to construct and utilize this versatile custom time-lapse microscopy and analysis system and for its application to several types of cell motility experiments.

Materials and methods

Time-lapse microscopy

Cells were prepared for time-lapse microscopy in three ways. For scratch assays, 9L rat gliosarcoma, U-87 human glioma, or MC3T3-E1 murine osteoblastic cells were grown to confluence in 35 mm plastic tissue culture dishes. Confluent monolayers were ''wounded'' in serum-free media by introducing scratches with a sterile 1 ml or 200 µl pipettor tip. Any treatments were then applied to wounded monolayers. Fluorescent vital labeled C6 glioma cells were plated at low density either on 35 mm culture dishes with a glass coverslip bottom insert (MatTek Corporation), or onto confluent NIH 3T3 cells pre-plated onto these dishes. Some experiments involved 3T3 cells that were stably transfected with an expression plasmid encoding the NgCAM/L1 adhesion molecule (kindly provided by Dr. Marty Grumet).

Cultures were placed into a custom culture chamber mounted on a ProScan II automated stage (Prior Scientific) on a Nikon TE-2000E microscope (Fig. 1). Temperature was maintained at 37°C by a combination of a warm air temperature controller (Air Therm; World Precision Instruments) and thermoelectric warming with an optical temperature-controlled stage insert (Thermo Plate; Tokai Hit, Japan). The atmosphere within the chamber was kept at 5% CO_2/95% air using a gas injection controller (Forma Scientific). A Photometrics CoolSnap ES CCD camera (Roper Scientific, Inc.) was used to capture images over the course of the experiment. The system was controlled using MetaMorph

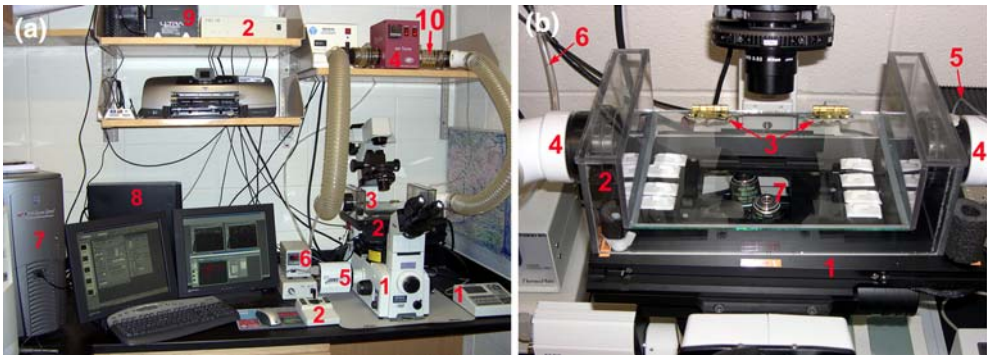

Fig. 1 Custom time-lapse microscopy apparatus components. This system is based on a standard automated inverted microscope with phase contrast and epifluorescence illumination. Phase contrast optics were chosen over other types because nuclei and fine cellular details can be seen clearly, and they are compatible with plastic tissue culture dishes and glass coverslips. Objectives (20× and 40×) contain correction collars so that they can be adjusted to compensate for the thickness of the dish or slide. The 12-bit cooled monochrome CCD camera is suitable for both phase contrast and fluorescence. The automated stage contains an optical sensor to improve accuracy of travel. (**a**) Time-lapse microscopy system. (1) Fully-automated Nikon TE-2000E with epifluorescence and external controller, (2) Prior ProScan II flat-top automated stage, stage controller, and joystick, (3) incubator chamber, (4) WPI temperature controller, (5) Photometrics CoolSNAP ES CCD camera, (6) Tokai Hit stage insert warmer controller, (7) custom 3 GHz computer with 2 gigabytes of RAM, 2 hard drives, dual monitors, and MetaMorph Premier software, (8) uninterruptible power supply capable of running entire system, (9) external USB backup hard drive, (10) CO_2 sensor for CO_2 injection system that is out of view. The stage contained a custom thermal plate warmer insert instead of a standard open slide or plate holder. The insert consisted of approximately coverslip-thick glass heated to a set temperature (37°C) by thermoelectric warming. This resulted in a transparent stage surface large enough for a multiwell tissue culture plate or any configuration of smaller plates, yet maintained a constant temperature at the sample surface. A small incubator chamber box could, thus, be designed to sit atop the stage and could be disconnected and removed easily, rather than awkwardly enclosing the whole microscope like some commercial systems. Warmed air was circulated through the chamber by large diameter hoses connected to the air warmer using plastic plumbing fittings and adapters. The remote temperature sensor was placed in the air outflow hose. CO_2 was injected into the chamber using an external CO_2 injector controller of which the sensor ''block'' was removed from its case and placed inline with the air flow of the chamber. The correct CO_2 injection pressure was empirically determined so that when the injector was set to 4% CO_2, the short burst of CO_2 resulted in a transient rise in the chamber to 6%. Thus, the CO_2 levels in the chamber fluctuated between 4% and 6%, averaging to the desired 5% CO_2 level. This was further confirmed by the correct orange-red color of the phenol red indicator dye in the culture media of samples in the chamber. Our development and testing of this custom incubator chamber configuration ultimately resulted in one that is more convenient, much more versatile, and several-fold less costly than current commercial configurations. It also allows direct parallel comparison between different desired experimental treatments while maintaining desired constant environmental conditions. MetaMorph software controlled the automated functions of the microscope and acquisition of images well. (**b**) Custom incubator chamber. (1) Prior automated stage, (2) clear plastic stage-top incubator chamber, (3) rear hinges securing glass incubator lid to plastic chamber, (4) plastic fittings for warmed air inflow (left) and outflow (right) of chamber, (5) lead for thermal sensor inserted into warm air outflow fitting, (6) tubing for CO_2 injection into air inflow side of chamber, (7) clear glass plate warmer stage insert

Premier Software (Molecular Devices Corporation), and images were collected using a Nikon CFI Plan Fluor ELWD DM 20× C Ph1 (correction collar 0–2 mm; 0.45 NA) objective lens at areas of interest on each plate at 5 min intervals for approximately 20 h. Illumination for phase contrast images contained a green filter inline. Fluorescent illumination was with a standard 100 watt mercury vapor lamp with an ND4, ND8, or no neutral density filter inline. Fluorescence exposure times ranged from 500 ms to 1,000 ms. Experiments usually consisted of collecting images from several areas of interest in each dish from three or four dishes to result in a total of several thousand images per experiment. Images from each location were separated into their own image stacks and converted into an avi movie at a speed of 15 frames per second for viewing, which corresponded to a time compression of approximately 1 h of experiment into 1 s of video.

Cell motility measurements

Motility of cells was measured after collection of sequential time-lapse images. Analyses were performed on sequential phase contrast images with MetaMorph software manually using the ''Track Points'' feature with individual nucleoli serving as imaging targets. This proved to be an easily identifiable and stable intracellular marker. The automatic ''Track Objects'' feature was used for fluorescent images with the search box surrounding the entire cell in some cases or fluorescent intracellular puncta in other cases. Automatic tracking with the Track Objects feature was not possible with phase contrast images in scratch assays because cell boundaries did not retain distinct contrast. Tracking by both manual Track Points or automatic Track Objects methods resulted directly in tabulation of data in a MetaMorph file of multiple motility parameters including object coordinates, distance traveled from last timepoint, velocity from last coordinate, absolute angle, and distance to origin in a straight line. Tabulated data were exported into Microsoft Excel, graphed, and evaluated statistically using Student's two-tailed *t*-test. DeltaGraph 5.6 (Red Rock Software) was also used for some analyses. The conversion factor for measured pixels to microns (0.46 for 20× objective) was determined by tracking using a Nikon stage micrometer.

Vital fluorescent labeling

Qtracker™ cell labeling was accomplished by following the manufacturer's directions using the Qtracker® 565 Cell Labeling Kit (Quantum Dot Corp.). Cells were incubated in Qtracker label mixture for 1 h in suspension at 37°C. Cells were plated on uncoated 35 mm MakTek coverslip-bottomed dishes, placed in the incubator overnight, and experiments were started the next day. Qtracker labeled cells contained extremely bright intracellular fluorescent puncta that were compatible with the MetaMorph automatic tracking feature. The filter cube used for evaluation of Qtracker contained a 505 nm dichroic mirror, a 510 nm long-pass emission filter, but contained interchanged excitation bandpass filters of differing wavelengths (400–500 nm, 420–500 nm, and 450–500 nm; Chroma Technology Corporation).

DiO cell membrane labeling was accomplished by incubating trypsinized C6 cells in a solution of 100 μg/ml DiO (3,3′-dioctadecyloxacarbocyanine perchlorate; Molecular Probes/Invitrogen) in normal culture medium (DMEM with 10% serum) similarly to that in Galileo et al. (1991). Cells were incubated for 1 h at 37°C, rinsed, and plated in 35 mm MatTek dishes. Cells were allowed to adhere overnight, during which time this membrane label was internalized and was visible as intracellular puncta. The filter cube used for DiO experiments was the Nikon EN GFP HQ BP cube with a 450–490 nm excitation filter, 495 nm dichroic mirror, and a 500–550 nm emission filter.

Green fluorescent protein (GFP) labeling was accomplished by using a recombinant lentiviral vector that encoded GFP and puromycin resistance (kindly provided by Dr. John Kappes, Univ. of Alabama). C6 cells were transduced with the GFP vector and selected to homogeneity using puromycin. C6/GFP cells were plated on the MatTek dishes as described above. The filter cube used for GFP experiments visualization was the same as for DiO.

Cell Tracker™ Green labeling was accomplished by Cell Tracker Green CMFDA (5-chloromethylfluorescein diacetate; Molecular Probes/Invitrogen) according to the manufacturer's directions. This molecule readily crosses the plasma membrane of intact cells and is retained intracellularly after reacting with cytoplasmic thiols. Cells were labeled in suspension with 5 μM reagent for 45 min at 37°C, rinsed, plated on MatTek dishes, and used the following day for experiments. The filter cube used for Cell Tracker Green experiment visualization was the same as for DiO and GFP.

Results

High-resolution time-lapse microscopy

The significance of observing and quantitating cell movements at closely spaced time intervals can be seen in Fig. 2. As a population of indi-

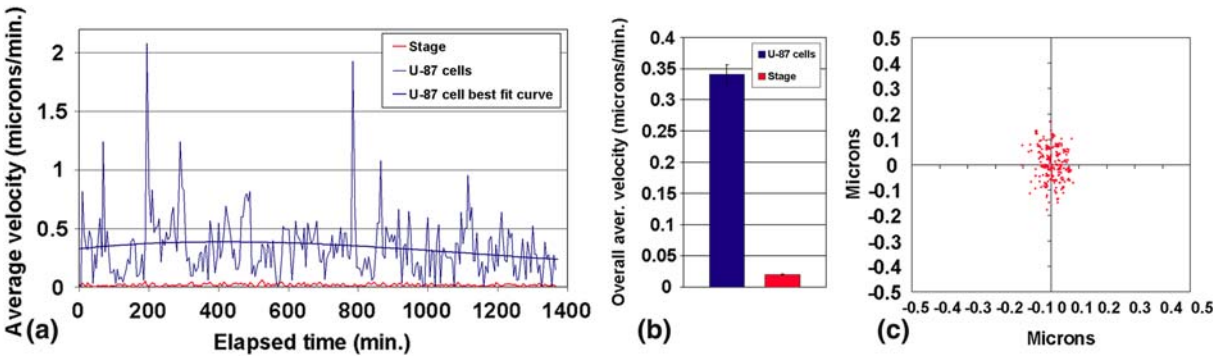

Fig. 2 High-resolution time-lapse microscopy. (**a**) Average velocity of a population of U-87 glioma cells treated with a stimulating antibody in a scratch assay experiment, plotted with stage accuracy data from (**c**) as velocity with 5 min time intervals. Shown is the 3rd-order polynomial curve of best fit for U-87 cell velocity. (**b**) Overall average of all U-87 cell and stage accuracy velocities. (**c**) The automated stage was programmed to travel to several distinct coordinates several centimeters apart. Sequential images were collected every 5 min for 23 h and at one coordinate a stationary mark on the tissue culture dish was tracked with the MetaMorph Track Object feature to evaluate the stage's ability to return to the exact programmed coordinate (graph origin). Plotted are 276 tracked points. Bars shown are SEM

vidually tracked U-87 cells migrates, their averaged velocity varies substantially at any particular timepoint (Fig. 2a, blue graph). A curve of best fit can approximate the overall average velocity of the migrating cells if the migration rate is fairly constant, as is the case here. However, neither the best fit curve nor the single overall velocity value (Fig. 2b) accurately represents the range of transient velocities at which cells can move. Even averaged velocities of a small population of cells can vary five-fold over average values at specific timepoints. Rare peak values of migration velocity (max. and min.) are obscured by overall averaged values, but may be an important component of the cell behavior of interest.

The custom time-lapse microscopy system we designed and assembled has resulted in collection of parallel time-lapse images under a wide variety of conditions. When tested for its ability to return to a single programmed coordinate, the stage returned to an average of 0.065 ± 0.002 μm (SEM) with a range of 0.001–0.178 μm (Fig. 2c). When velocity errors due to the stage movement inaccuracy were plotted with velocities of migrating cells (Fig. 2a, red graph), they were a constant but minor component of measured velocities. Overall average velocity error due to stage inaccuracy was calculated to be 0.020 ± 0.001 μm/min (SEM), which is small compared to the migrating cells (0.341 ± 0.016 μm/min SEM; Fig. 2b). These errors in stage movement are mostly imperceptible in time-lapse movies and, thus, the high-throughput advantage of the automated stage outweighs the disadvantage of the negligible inaccuracy.

A novel approach was taken for the cell incubator chamber that was used for time-lapse studies and it is described in Fig. 1. This design allowed cells to be analyzed in a variety of tissue culture dishes and plates, including 35 mm, 60 mm, 10 cm, multiwell plates, chamber slides, and small T-flasks. This makes our design much more versatile than currently available commercial systems. We initially found that vibrations generated by the motors in the automated stage would cause the dishes to move slightly on the Tokai Hit insert over the course of the experiment. This was easily remedied by brushing a thin coat of rubber cement along the bottom edge of the dish and allowing it to dry before plating cells. This created a non-skid surface that prevented dish movement.

The super scratch assay

A successful application of our time-lapse microscopy and quantitation of motility has been to the conventional ''scratch'' or ''wound healing'' assay. This simple semi-quantitative assay

has been improved here to be a highly quantitative assay (hence ''*Super Scratch*'' assay) capable of providing detailed information about multiple motility parameters. An example of the improvement in accuracy is shown in Fig. 3. Lines can be drawn to represent the beginning and ending of the scratch edges from which the average distance that the cell front advances can be measured. This ''line method'' measures the greatest extent to which the cell margin has migrated to fill in the scratch. This appears to be a reasonable approach for cells that migrate in relatively straight trajectories as a unified front, such as for 9L glioma cells (Fig. 3a) or even transfected 9L cells expressing an ectopic adhesion molecule (Fig. 3b). Surprisingly, when the distance of migration was calculated, the approximated line estimates were considerably

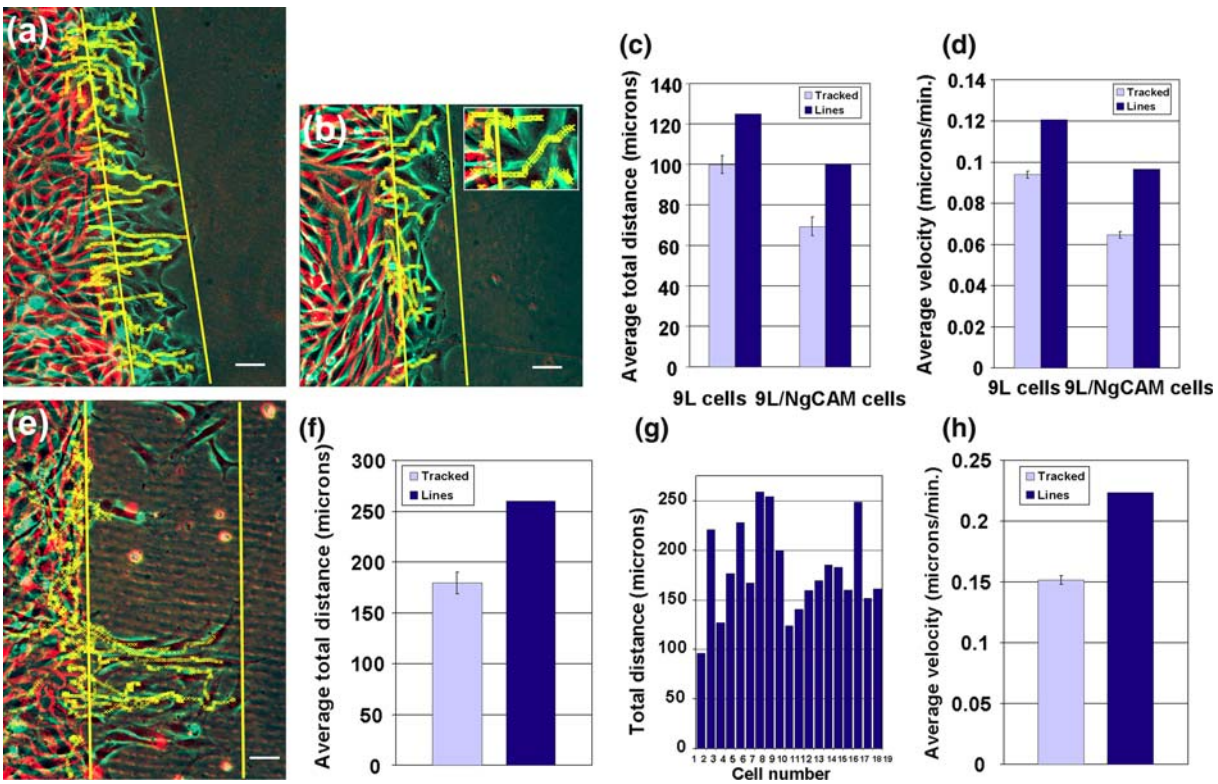

Fig. 3 Super Scratch assay comparison with conventional scratch assay. (**a**) First phase contrast image of 208 sequential images of a 9L glioma scratch was pseudocolored red, last image in series was pseudocolored green, and the images were superimposed. Yellow straight lines delimit the borders of the scratch at the beginning and end of the experiment (17 h). Yellow curved lines are series of 208 yellow ''X''s that indicate the position of each tracked cell (24 total cells) in each sequential image analyzed in the *Super Scratch* assay, thus showing the migration paths. (**b**) Same as in (**a**), but for 9L cells transfected with NgCAM expression plasmid (9L/NgCAM cells). A total of 15 cells were tracked. Inset is magnification of region to the left to better visualize tracks of yellow ''X''s. (**c**) Distances were measured between straight yellow lines for conventional scratch assay, and distances of each cell path were averaged for the *Super Scratch* assay. Bars for tracked cells are SEM. (**d**) Velocities of all tracked cells for all timepoints were averaged for the *Super Scratch* assay, and velocities of conventional scratch assays were calculated by dividing the distance between straight lines by experiment length. (**e**) Same procedure as in (**a**) and (**b**) for MC3T3-E1 osteoblasts treated with 1 μM lysophosphatidic acid (LPA). Note that 3 of the 19 tracked cells have migrated backwards into the confluent cell monolayer, some cells migrated parallel to the scratch, and cells at the top of the image by the right (endpoint) line migrated there from outside the field of view. (**f**) Distances of cells shown in (**e**) determined by the conventional scratch and *Super Scratch* methods. Bar is SEM. (**g**) Individual path distances of the 19 tracked cells shown in (**e**). (**h**) Velocities for osteoblasts in (**e**) calculated as in (**d**). Bar for tracked cells is SEM. Micron bars, 50 μm

greater than the averaged distances calculated by tracking individual cell paths at the wound edge using object tracking software (Fig. 3c).

The apparent inaccuracy for gliomas was a 25% overestimate (100 μm tracked vs. 125 μm by the line method), and for transfected gliomas was a 45% overestimate (69 μm tracked vs. 100 μm by the line method). The overestimates by the line method are due to the fact that not all cells of the advancing front migrate equally fast or far as the most advanced cells, which is where the second line was drawn. The greater inaccuracy for transfected cells might be attributed to their more irregular paths (i.e. less straight; see yellow "X"s). The difference in migration distance caused by the adhesion molecule expression as determined by cell tracking was a 31% reduction of control distance (31 μm/100 μm), compared to a 20% reduction (25 μm/125 μm) as determined by the line-method. These line-method inaccuracies in distance, then, are also translated into discrepancies in velocity when conversions are done using the duration of the experiment for the line method (Fig. 3d). Thus, a substantial misrepresentation of cell behavior can result from measurements made by distance measurements between advancing fronts of cells in a conventional scratch assay.

Cell migration during the scratch assay also can lead to the appearance of a very irregular border of advancing cells. In such cases, a line can still be drawn at the end of the experiment that is parallel to the initial scratch border delimiting the extent of the farthest migrating cells (Fig. 3e). However, it seems reasonable to predict that measurements using the line-method might not be accurate under this condition. The approximated distance of migration in such a case determined by the line-method was a large over-estimation (44%; 260 μm by line-method vs. 180 μm by tracking; Fig. 3f), similar to that for transfected cells with a more regular border. Individual tracked cell migration distances varied over 2.5-fold (Fig. 3g). Since the treatment conditions employed here were expected to induce random motility (chemokinesis) as opposed to directed cell movement (chemotaxis), it was not surprising that several cells migrated backwards into the monolayer (Fig. 3e; leftmost yellow paths). Average migration velocity was also an over-estimate by the line-method (Fig. 3h). Thus, actual cell migratory behavior can be inaccurately represented by methods employing gross measurements, and inspection of an endpoint image does not reliably assess the cell behavior up to that point. Although such a conclusion might be suspected, the high resolution data gathered by the tracking methods clearly demonstrates this.

Cell migration dynamics

The conventional scratch assay, when quantitated, is often scored as a single distance measurement. Deduction of migration velocity from a single measurement must either assume that migration rates do not change over the course of the experiment (i.e., velocities are constant), or ignore potential changes. We found that this assumption was not true for certain experimental cell treatments, as well as for some control untreated cells. This can be appreciated when either average cumulative distances or velocities are plotted against elapsed time. For distance versus time, a line represents constant velocity whereas a curve represents changing velocity. For instance, when osteoblasts were continuously drug treated, their velocity increased transiently (e.g., from 150 min to 600 min in Fig. 4b), but then diminished to approach control cell levels (Fig. 4a, b). This resulted in a large difference in endpoint cumulative distance (Fig. 4a), but neither endpoint distance nor a single averaged velocity value would accurately reflect the changes in cell migration rates that took place. Antibody treatments also have resulted in changes in migration kinetics (data not shown).

Such dynamic changes in velocity do not always occur after experimental treatments, however. Fluorescently labeled glioma cells (with Qtracker™; see below) tracked on monolayers expressing an adhesion molecule were slowed in velocity, but the change was rather constant throughout the experiment (Fig. 4c, d). This is an example where reduction of velocities to a single overall average (Fig. 4e) would be indicative of cell behavior. We also previously found that glioma cells transfected with DNA encoding an adhesion molecule exhibited a constant decreased

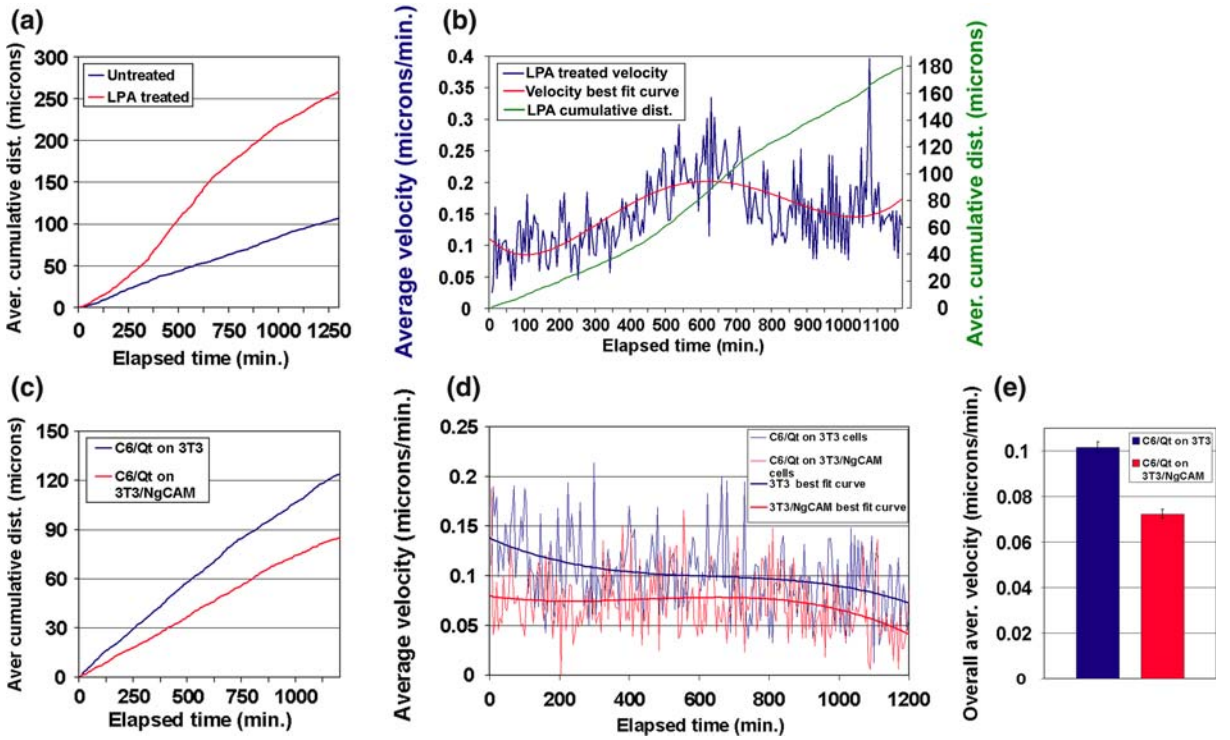

Fig. 4 Cell migration dynamics. (**a**) MC3T3-E1 cells were tracked in the scratch assay as either untreated or treated with 2.5 μM LPA. Plotted are the average cumulative distances at each 5-min interval (260 total). Note that untreated cells migrated with a fairly constant velocity ($y = 0.4184x + 0.1024$; $R^2 = 0.9983$), but treated cells migrated with a changing velocity ($y = 1E\text{-}07x^4 - 9E\text{-}05x^3 + 0.0189x^2 - 0.0877x + 3.8552$; $R^2 = 0.9996$). (**b**) MC3T3-E1 cells were tracked in the scratch assay as either untreated or treated with 1 μM LPA. Plotted is the average velocity (blue) with 3rd-order curve of best fit (red) and average cumulative distance. Average cumulative distance is shown in green. (**c**) C6 cells labeled with fluorescent Qtracker were plated on either 3T3 cells (blue) or NgCAM transfected 3T3 cells (red), tracked, and average cumulative distances are plotted. Note that reduced velocity of C6/Qt cells on 3T3/NgCAM cells is constant. (**d**) Same cells in. (**c**) plotted as average velocities over time with 3rd-order curves of best fit. (**e**) Overall average velocities of C6/Qt cells shown in (**d**). Bars indicate SEM

migration velocity (Cretu et al. 2005). Thus, our method of quantitation and analysis of cell migration rates over closely spaced time points allowed detection of dynamic changes in migration velocity, such as initial or subsequent increases or decreases, or of constant velocity. The possibility of such changes in velocity so far has not been considered by others in conventional cell migration analyses, but clearly should be.

Time-lapse using fluorescent vital labeling

Fluorescent vital labeling is not necessary for tracking cells in scratch assays or when migrating randomly on coated or plain plastic or glass surfaces. However, if cells of interest are plated on a cell monolayer or a tissue slice, then single cells of interest are not discernable with normal optics. To overcome this limitation, several different methods of vital fluorescent cell labeling were evaluated for their suitability in time-lapse experiments. Of the four methods evaluated, three could be used successfully with our system: Qtracker™ 565, DiO, and GFP expression. The results are summarized in Table 1. A fourth method using Cell Tracker™ Green was found not to be satisfactory due to extreme bleaching and, thus, disappearance of the fluorescent label under illumination conditions similar to that for the other labeling methods. The other methods

Table 1 Properties of vital fluorescent labeling agents for time-lapse microscopy

	GFP expression	DiO	Qtracker™	Cell tracker™ green
Detectable fluorescence	Moderate throughout	High but tapered off	High throughout	Moderate at first, bleached rapidly
Bleaching	Low	Moderate	Very low	Extreme and rapid
Cell viability	High with ND filters	High with ND filters	High with ND filters	Unknown due to bleaching
Usable conditions	ND4 filter 5 min intervals	ND8 filter 12.5 min intervals	ND8 filter 5 min intervals 450–500 nm excitation	None with our system

could be used under specific combinations of illumination intensity and time interval. Initial assessment was performed at standard time intervals of 5 min, with full epifluorescent illumination (blue light, no ND filter), and a 20-h experiment duration. At each time point, the cells were subjected to epifluorescent illumination for a few seconds, which was determined by the software's ability to control the hardware. We found that conditions had to be optimized for each labeling method to enable visualization of labeled cells without adverse effects due to repeated exposure to blue light.

For cells expressing GFP label, full fluorescence illumination intensity was not satisfactory and resulted in lowered initial migration rates and death of cells (Fig. 5a–d) compared to phase illumination (Fig. 5a). This assay was performed with non-confluent cells undergoing non-directed random migration in a glass bottom culture dish. To determine if GFP expression itself or illumination intensity was responsible for slowed migration and death, cells with and without GFP expression were analyzed similarly with full illumination intensity and with a neutral density filter in the illumination path. All samples including cells with or without GFP label were adversely affected by full illumination (Fig. 5e). Insertion of an ND4 filter inline with the epifluorescent light source (25% illumination intensity) resulted in stable motility of both labeled and unlabeled cells over an 18 h experiment (Fig. 5f). Thus, cells were vulnerable in our experiments to repeated over-illumination with blue light, but GFP was a useful vital label when excitation intensity was reduced by a factor of four.

DiO carbocyanine dye labeling was not useful under the above conditions for GFP, and required even less intense and less frequent illumination. Stable migration velocities were found with 12.5 min time intervals, ND8 filter, and 17-hour experiment duration (Fig. 5g). The day after labeling cells, DiO was visible as intracellular puncta (Fig. 5h), which could be used to track cells automatically. Intracellular puncta form as cells endocytose labeled plasma membrane and incorporate label into endocytotic vesicles. These large intracellular vesicles were stable inside cells and could be used for tracking cell migration using the Track Objects feature. Viewing movies compiled from time-lapse images revealed that there was noticeable, but tolerable, DiO photobleaching over the course of the experiment. Thus, DiO is useful for time-lapse experiments under appropriate conditions. But, it evidently was toxic when illuminated with blue light that normally would not affect unlabeled cells (ND4 filter, 5 min intervals) and so 12.5 min intervals and ND8 filter needed to be used.

Qtracker™ 565 labeling was evaluated using fluorescence filter cubes with three different increasingly narrow excitation bandpass ranges (see Methods). This was done because the cadmium selenide nanocrystal core of the quantum dot absorbs mostly ultraviolet light, which is toxic to living cells. We found that the two shorter wavelength excitation bandpasses resulted in cell death (data not shown) and that only the 450–500 nm excitation resulted in viable cells under our conditions of repeated time-lapse exposure. This label was still extremely bright and allowed the use of an ND8 filter in the excitation pathway, and no detectable photobleaching occurred.

Qtracker™ labeling was applied to the analysis of glioma cell behavior on normal NIH 3T3

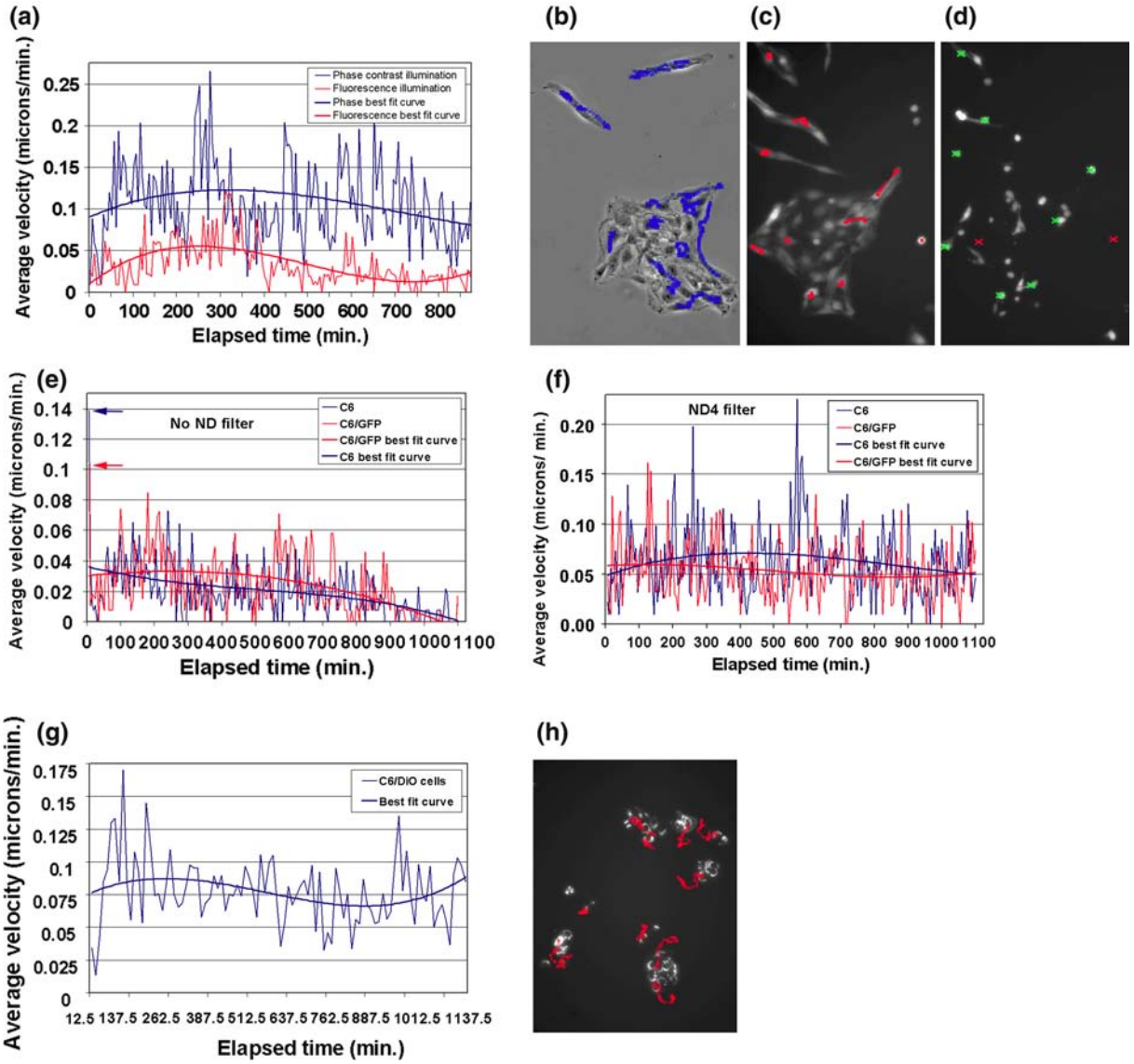

Fig. 5 Evaluation and application of vital fluorescent labeling methods. (**a**) C6 cells were labeled by infection with a GFP-encoding retroviral vector. Images were collected using either phase contrast (blue graph) or fluorescent (red graph) illumination. Plotted are average velocities over time and 3rd-order curves of best fit. (**b**) Initial image of 10 C6/GFP cells tracked in (**a**) with phase contrast and their migratory paths shown in blue ''X''s. Each ''X'' represents cell position in a sequential image. (**c**) Initial image of C6/GFP cells tracked in (**a**) with fluorescence (450–490 nm) illumination without an ND filter, and their migratory paths shown in red ''X''s. (**d**) Last image of C6/GFP cells tracked in (**b**) showing ultimate position denoted by a green ''X''. The two red ''X''s denote cells that have lysed before the end of the experiment ended and no longer exhibited GFP fluorescence. Note also the general rounded appearance of the cells. (**e**) C6 and C6/GFP cells both were illuminated with fluorescent (450–490 nm) light with no ND filter and tracked over time. Graphed are average velocities and 3rd-order curves of best fit. Note that both cell types exhibited initial velocities over 0.1 μ/min (arrows), but immediately and drastically slowed in migration rate, and died by the end of the experiment. (**f**) C6 and C6/GFP cells both were illuminated with fluorescent (450–490 nm) light with an ND4 filter and tracked over time. Graphed are average velocities and 3rd-order curves of best fit. Note that both cell types exhibited stable velocities throughout the experiment. (**g**) C6 cells were labeled with DiO and illuminated with blue light (450–490 nm) with an inline ND8 filter at 12.5 min intervals and tracked over 17 h. The average cell velocity remained stable as shown by the 3rd-order curve of best fit. (**h**) Initial image of the 10 cells tracked in (**g**) and the paths that they migrated shown in red

cell monolayers and on monolayers expressing cell surface adhesion molecule NgCAM/L1 (Fig. 4c, d). Labeled cells were extremely bright and were clearly visible through the monolayers with an ND8 filter. Cell movements were tracked as they migrated randomly about on the cell monolayers. C6/Qt cell migration velocities are shown in Fig. 4d where a consistent decrease was apparent for cells on the 3T3/NgCAM monolayers throughout the experiment. When reduced to overall average velocity values, cell migration was reduced by 29% and was highly significant (Fig. 4e; $P << 0.001$). Thus, fluorescent vital labeling allowed cell motility to be tracked and quantitated in response to a single cell surface molecule (NgCAM/L1) when presented in the context of a living cellular substratum (3T3 cells).

Discussion

The methods currently in use to measure cell movements often lack ability to provide answers to specific questions about migrating cells. For instance, it is difficult or impossible to approach questions such as: What are the actual velocities of untreated cells versus those treated with a drug? What is the range of individual velocities within a cell population? What are the paths that the individual cells took? Do the migration rates of the treated cells change over time? These questions are important to answer in a detailed analysis of cell migration. Our methods have resulted in higher spatial precision and higher temporal resolution and, therefore, more accurate representation of cell motility behavior than heretofore. A requisite for precise quantitation of cell movements is that measurements be accurate, especially when the stage travels between several points of interest at each time interval. The automated system described here is stable and accurate and introduces remarkably small errors to measured distances and velocities for stage movements that approach 10 cm.

We have presented several examples of how our time-lapse microscopy system and application of object tracking software to migrating cells overcame conventional limitations. One of our main focuses was to refine the commonly used scratch or wound healing assay into a highly quantitative *Super Scratch* assay. The scratch assay before this work had not progressed beyond a single or few timepoint assay where measurements were made of distance between edges (Maschler et al. 2005; Zhu et al. 2004; Pratt et al. 2005; Wadham et al. 2003; Besson et al. 2004; Cretu et al. 2005; Hoang et al. 2004; John et al. 2004; Ray et al. 2003; Lynch et al. 2005; Yarrow et al. 2004), number of cells entering a defined area (Petridis et al. 2004; Nishio et al. 2005; Zhu et al. 2004; Piccolo et al. 2002; Robinet et al. 2005; Raftopoulou et al. 2004; Zhu et al. 2005), or qualitative assessment without quantitation (Gavert et al. 2005; Yoshida et al. 2004; Zhang et al. 2005; Herren et al. 2001; Lee et al. 2004; Motegi et al. 2003; Laurent-Matha et al. 2005; Miao et al. 2005). We have shown that such a method of analysis is not as accurate a representation of cell migration as tracking individual cells starting from the advancing front of the wound. ''Average'' distances and velocities calculated by using the line or similar method, although they provide a measurement of the extent to which a gap is filled in by cells, cannot be used with certainty to accurately measure a cell population's actual average migration distance or velocity. And since experimental treatments can affect direction of migration and other cell behavior, an inaccurate conclusion might be drawn about cell migration distance, direction, or velocity using the line-method or any method measuring only the advancement of the leading edge at the experiment endpoint. Such analyses are based on the several assumptions that cells maintain relatively straight trajectories, that cells at the advancing front are indicative of those cells behind them, that motility kinetics do not change throughout the time period, and that significant cell division does not take place, some or all of which may be false within a given experiment. Here, examples are shown where most of these assumptions would not have been valid, and we speculate that this may often be the case. Thus, conclusions made in other studies without further analysis of individual cell migration velocity or direction might be subject to error.

Others have tracked individual cells over periods of time, but have reported only overall averaged velocity values and not plotted values over time (Edme et al. 2002; Harms et al. 2005; Huang et al. 2003; Six et al. 2004; Sun et al. 2004). The highly quantitative *Super Scratch* assay has been useful already for determining the effects on cell behavior after drug treatment, transfection, and antibody treatment. In two of these treatments, the effect on cell velocity changed with time, which underscores the ability of our assay to reveal previously unknown dynamics of cell migration. Using this assay, delays in the effects of drug treatment on migration as well as desensitization (i.e., return to control values) of cells to a treatment can be detected. This method provides the means to study treatments that might have effects on migration where the changes in kinetics themselves are the most important results. By analogy, then, the *Super Scratch* assay may be to the scratch assay what real-time PCR is to PCR.

This work provides a starting point for performing time-lapse experiments and for using several vital fluorescent labeling methods. It improves upon existing time-lapse video microscopy systems currently in use in that it enables monitoring of cells over long experimental durations. The assessment of the several labels and conditions presented in Table 1 should allow selection of an appropriate label and experimental conditions for other investigators. This evaluation was necessary for our application of motility analyses on cell monolayers, but can also be applied to migration on tissue slices, or to determining cell behaviors when two or more cell populations with different color labels are mixed. A supplementary document detailing the construction of the incubator chamber will be provided upon request and will allow investigators to determine whether this, or a commercial incubator system, is most suitable for their needs.

Acknowledgements This work was supported by grants from NIH to D.S.G. (NS040317), to J.K. (NS049523), and to N.J.K. (HD042066). We gratefully acknowledge that the filter cube with custom excitation bandpass filters was provided by Chroma Technology Corporation. J. Fotos and V. Patel were awarded undergraduate research fellowships through grants to the Univ. of Delaware from the Howard Hughes Medical Institute and the Ronald E. McNair Program. We gratefully thank Dr. John Kappes for the GFP lentiviral vector construct and Dr. Marty Grumet for the NgCAM/L1 cDNA construct.

References

Besson A, Gurian-West M, Schmidt A, Hall A, Roberts JM (2004) p27Kip1 modulates cell migration through the regulation of RhoA activation. Genes Dev 18:862–876

Cretu A, Fotos JS, Little BW, Galileo DS (2005) Human and rat glioma growth, invasion, and vascularization in a novel chick embryo brain tumor model. Clin Exper Metas 22:225–236

Edme N, Downward J, Thiery JP, Boyer B (2002) Ras induces NBT-II epithelial cell scattering through the coordinate activities of Rac and MAPK pathways. J Cell Sci 115:2591–2601

Endo Y, Wolf V, Muraiso K, Kamijo K, Soon L, Uren A, Barshishat-Kupper M, Rubin JS (2005) Wnt-3a-dependent cell motility involves RhoA activation and is specifically regulated by dishevelled-2. J Biol Chem 280:777–786

Galileo DS, Gee AP, Linser PJ (1991) Neurons are replenished in cultures of embryonic chick optic tectum after immunomagnetic depletion. Dev Biol 146:278–291

Gavert N, Conacci-Sorrell M, Gast D, Schneider A, Altevogt P, Brabletz T, Ben-Ze'ev A (2005) L1, a novel target of beta-catenin signaling, transforms cells and is expressed at the invasive front of colon cancers. J Cell Biol 168:633–642

Harms BD, Bassi GM, Horwitz AR, Lauffenburger DA (2005) Directional persistence of EGF-induced cell migration is associated with stabilization of lamellipodial protrusions. Biophys J 88:1479–1488

Herren B, Garton KJ, Coats S, Bowen-Pope DF, Ross R, Raines EW (2001) ADAM15 overexpression in NIH3T3 cells enhances cell–cell interactions. Exp Cell Res 271:152–160

Hoang MV, Whelan MC, Senger DR (2004) Rho activity critically and selectively regulates endothelial cell organization during angiogenesis. Proc Natl Acad Sci USA 101:1874–1879

Huang C, Rajfur Z, Borchers C, Schaller MD, Jacobson K (2003) JNK phosphorylates paxillin and regulates cell migration. Nature 424:219–223

John GR, Chen L, Rivieccio MA, Melendez-Vasquez CV, Hartley A, Brosnan CF (2004) Interleukin-1beta induces a reactive astroglial phenotype via deactivation of the Rho GTPase-Rock axis. J Neurosci 24:2837–2845

Laurent-Matha V, Maruani-Herrmann S, Prebois C, Beaujouin M, Glondu M, Noel A, Alvarez-Gonzalez ML, Blacher S et al (2005) Catalytically inactive human cathepsin D triggers fibroblast invasive growth. J Cell Biol 168:489–499

Lee CC, Putnam AJ, Miranti CK, Gustafson M, Wang LM, Vande Woude GF, Gao CF (2004) Overexpression of sprouty 2 inhibits HGF/SF-mediated cell growth, invasion, migration, and cytokinesis. Oncogene 23:5193–5202

Lynch L, Vodyanik PI, Boettiger D, Guvakova MA (2005) Insulin-like growth factor I controls adhesion strength mediated by alpha5beta1 integrins in motile carcinoma cells. Mol Biol Cell 16:51–63

Maschler S, Wirl G, Spring H, Bredow DV, Sordat I, Beug H, Reichmann E (2005) Tumor cell invasiveness correlates with changes in integrin expression and localization. Oncogene 24:2032–2041

Miao H, Strebhardt K, Pasquale EB, Shen TL, Guan JL, Wang B (2005) Inhibition of integrin-mediated cell adhesion but not directional cell migration requires catalytic activity of EphB3 receptor tyrosine kinase. Role of Rho family small GTPases. J Biol Chem 280:923–932

Motegi S, Okazawa H, Ohnishi H, Sato R, Kaneko Y, Kobayashi H, Tomizawa K, Ito T et al (2003) Role of the CD47-SHPS-1 system in regulation of cell migration. EMBO J 22:2634–2644

Moyano JV, Maqueda A, Casanova B, Garcia-Pardo A (2003) Alpha4beta1 integrin/ligand interaction inhibits alpha5beta1-induced stress fibers and focal adhesions via down-regulation of RhoA and induces melanoma cell migration. Mol Biol Cell 14:3699–3715

Nishio T, Kawaguchi S, Yamamoto M, Iseda T, Kawasaki T, Hase T (2005) Tenascin-C regulates proliferation and migration of cultured astrocytes in a scratch wound assay. Neuroscience 132:87–102

Petridis AK, El-Maarouf A, Rutishauser U (2004) Polysialic acid regulates cell contact dependent neuronal differentiation of progenitor cells from the subventricular zone. Dev Dyn 230:675–684

Piccolo E, Innominato PF, Mariggio MA, Maffucci T, Iacobelli S, Falasca M (2002) The mechanism involved in the regulation of phospholipase Cgamma1 activity in cell migration. Oncogene 21:6520–6529

Pratt SJ, Epple H, Ward M, Feng Y, Braga VM, Longmore GD (2005) The LIM protein Ajuba influences p130Cas localization and Rac1 activity during cell migration. J Cell Biol 168:813–824

Raftopoulou M, Etienne-Manneville S, Self A, Nicholls S, Hall A (2004) Regulation of cell migration by the C2 domain of the tumor suppressor PTEN. Science 303:1179–1181

Ray RM, McCormack SA, Covington C, Viar MJ, Zheng Y, Johnson LR (2003) The requirement for polyamines for intestinal epithelial cell migration is mediated through Rac1. J Biol Chem 278:13039–13046

Robinet A, Fahem A, Cauchard JH, Huet E, Vincent L, Lorimier S, Antonicelli F, Soria C et al (2005) Elastin-derived peptides enhance angiogenesis by promoting endothelial cell migration and tubulogenesis through upregulation of MT1-MMP. J Cell Sci 118:343–356

Six EM, Ndiaye D, Sauer G, Laabi Y, Athman R, Cumano A, Brou C, Israel A, Logeat F (2004) The notch ligand Delta1 recruits Dlg1 at cell–cell contacts and regulates cell migration. J Biol Chem 279:55818–55826

Sun S, Wise J, Cho M (2004) Human fibroblast migration in three-dimensional collagen gel in response to noninvasive electrical stimulus. I. Characterization of induced three-dimensional cell movement. Tissue Eng 10:1548–1557

Wadham C, Gamble JR, Vadas MA, Khew-Goodall Y (2003) The protein tyrosine phosphatase Pez is a major phosphatase of adherens junctions and dephosphorylates beta-catenin. Mol Biol Cell 14:2520–2529

Yarrow JC, Perlman ZE, Westwood NJ, Mitchison TJ (2004) A high-throughput cell migration assay using scratch wound healing, a comparison of image-based readout methods. BMC Biotechnol 4:21

Yoshida H, Cheng W, Hung J, Montell D, Geisbrecht E, Rosen D, Liu J, Naora H (2004) Lessons from border cell migration in the Drosophila ovary: a role for myosin VI in dissemination of human ovarian cancer. Proc Natl Acad Sci USA 101:8144–8149

Zhang L, Deng M, Parthasarathy R, Wang L, Mongan M, Molkentin JD, Zheng Y, Xia Y (2005) MEKK1 transduces activin signals in keratinocytes to induce actin stress fiber formation and migration. Mol Cell Biol 25:60–65

Zhu N, Lalla R, Eves P, Brown TH, King A, Kemp EH, Haycock JW, MacNeil S (2004) Melanoma cell migration is upregulated by tumour necrosis factor-alpha and suppressed by alpha-melanocyte-stimulating hormone. Brit J Cancer 90:1457–1463

Zhu X, Jiang J, Shen H, Wang H, Zong H, Li Z, Yang Y, Niu Z et al (2005) Elevated beta1,4-galactosyltransferase I in highly metastatic human lung cancer cells. Identification of E1AF as important transcription activator. J Biol Chem 280:12503–12516